Food Research International 176 (2024) 113822

Contents lists available at ScienceDirect

Food Research International

journal homepage: www.elsevier.com/locate/foodres

A comprehensive study from the micro- to the nanometric scale: Evaluation of chilling injury in tomato fruit (*Solanum lycopersicum*)

C.I. Acosta-Ramírez [a,b], I.D. Lares-Carrillo [a], L.E. Ayón-Reyna [c], M.E. López-López [c], M.O. Vega-García [c], J.G. López-Velázquez [c], G.F. Gutiérrez-López [b], U. Osuna-Martínez [d], E. García-Armenta [a,c,*]

[a] Facultad de Ciencias Químico Biológicas, Universidad Autónoma de Sinaloa, Ciudad Universitaria, Culiacán, Sinaloa 80013, Mexico
[b] Instituto Politécnico Nacional, Escuela Nacional de Ciencias Biológicas, Carpio y Plan de Ayala S/N, Ciudad de México 11340, Mexico
[c] Posgrado en Ciencia y Tecnología de Alimentos, Facultad de Ciencias Químico Biológicas, Universidad Autónoma de Sinaloa, Ciudad Universitaria, Culiacán, Sinaloa 80013, Mexico
[d] Laboratorio de Investigación en Farmacia, Farmacobiología y Toxicobiología, Facultad de Ciencias Químico Biológicas, Universidad Autónoma de Sinaloa, Ciudad Universitaria, Culiacán, Sinaloa 80013, Mexico

ARTICLE INFO

Keywords:
Tomato
Chilling injury
Digital image analysis
Fractal dimension
Multi-scale approach

ABSTRACT

Tomato fruit is susceptible to chilling injury (CI) during its postharvest handling at low temperature. The symptoms caused by this physiological disorder have been commonly evaluated by visual inspection at a macro-observation scale on fruit surface; however, the structure at deeper scales is also affected by CI. This work aimed to propose a descriptive model of the CI development in tomato tissue under the micro-scale, micro-nano-scale and nano-scale approaches using fractal analysis. For that, quality and fractal parameters were determined. In this sense, light microscopy, Environmental Scanning Electron Microscopy (ESEM) and Atomic Force Microscopy (AFM) were applied to analyse micro-, micro-nano- and nano-scales, respectively. Results showed that the morphology of tomato tissue at the micro-scale level was properly described by the multifractal behaviour. Also, generalised fractal dimension ($D_{q=0}$) and texture fractal dimension (FD) of CI-damaged pericarp and cuticle were higher (1.659, 1.601 and 1.746, respectively) in comparison to non-chilled samples (1.606, 1.578 and 1.644, respectively); however, FD was unsuitable to detect morphological changes at the nano-scale. On the other hand, lacunarity represented an appropriate fractal parameter to detect CI symptoms at the nano-scale due to differences observed between damaged and regular ripe tissue (0.044 and 0.025, respectively). The proposed multi-scale approach could improve the understanding of CI as a complex disorder to the development of novel techniques to avoid this postharvest issue at different observation scales.

1. Introduction

Tomato fruit (*Solanum lycopersicum*) is an important worldwide commodity owing to its versatile culinary use, benefits to human health and economic profits (Ali et al., 2020; Lares-Michel et al., 2018; Sandoval-Ceballos et al., 2021). The merchandising of this product includes their harvest at a breaker ripening stage and subsequent storage and transportation at refrigerated temperatures to control its ripening process, however, tomatoes are susceptible to a physiological disorder called chilling injury (CI) (Imahori et al., 2016). CI has been reported as a result of structural damage and biochemical modifications in the affected tissue, which have been related to metabolic changes producing variations in cell wall permeability, enzyme regulation, increase in cytosolic free calcium concentration, and others (Ding et al., 2019; Jha et al., 2019; Song et al., 2022). Consequently, CI represents a severe issue which causes alterations in fruit quality such as darkening, softening, pitting, water loss, abnormal ripening, and odour and flavour changes (Carvajal et al., 2015; Erkan et al., 2005); hence, it causes major economic losses. Several postharvest techniques have been employed to minimise this problem such as intermittent heat treatment, controlled atmospheres, chemical treatments and growth regulators (Ayón-Reyna et al., 2017; Pristijono et al., 2018; Zhu et al., 2016).

CI symptoms in tomatoes can be identified by visual inspection; however, structural damage may occur at deeper observation scales with

* Corresponding author at: Facultad de Ciencias Químico Biológicas, Universidad Autónoma de Sinaloa, Ciudad Universitaria, Culiacán, Sinaloa 80013, Mexico.
E-mail address: eva.garmenta@uas.edu.mx (E. García-Armenta).

https://doi.org/10.1016/j.foodres.2023.113822
Received 28 August 2023; Received in revised form 29 November 2023; Accepted 2 December 2023
Available online 3 December 2023

no visible symptoms at the macro-scale level. Hence, it is important to describe these structural changes triggered by CI to achieve more effective treatments that might act at micro- and nano-scales. In this sense, the description of CI at different observation levels has been studied in bell peppers, finding that this physiological disorder induced plasmolysis, collapsed cells and damaged organelles, which were detected based on the visual inspection of Transmission Electron Microscopy (TEM) images (Ge et al., 2019). Also, Besada et al. (2015) reported that microstructural changes [from Cryoscanning Electron Microscopy (Cryo-SEM)] in persimmon fruits under CI conditions consisted in the visual identification of increased intercellular spaces, cellular stress revealed by cells filled with soluble material and loss of cellular integrity. However, these evaluations were performed centred in the subjective visual observation of microscopy images. In this sense, it is necessary to develop standardised techniques to detect CI symptoms. For this, quantitative techniques such as the fractal approach have been applied to describe morphometric changes occurring in several food processes (García-Armenta & Gutiérrez-López, 2022). Fractals are a special case of figures that possess self-similarity and are characterised by their fractal dimension and a lacunarity parameter, which have been commonly determined by digital image analysis (Cáez Ramírez et al., 2017).

Therefore, the aim of this work was to propose a descriptive model of the CI development in tomato tissues under the micro-scale, micro-nano-scale and nano-scale approaches using fractal analysis.

2. Materials and methods

2.1. Plant material

Tomato fruit var. Saladette were acquired in a local market in Culiacan, Sinaloa, Mexico. Fruit were in a breaker ripening stage [according to the United States Department of Agriculture (USDA)] and were uniformly selected in size and colour with the absence of mechanical damage and fungal lesions.

2.2. CI induction

The experimental strategy involved the tomato storage based on a two-factor design: storage days and temperature. Fruit were disinfected by immersion in a NaClO solution (300 mg/L) for 3 min and stored at 12 °C (safe temperature) and 4 °C (CI conditions) for 12 days in a cold chamber, hermetically sealed without sunlight exposition. After that, fruit were subjected to a ripening stage of 7 days at 21 °C.

2.3. Evaluation of CI index

CI index was determined using a hedonic scale according to methodology reported by Vega-García et al. (2010) with some modifications. Visible symptoms were identified in tomato samples based on the following criteria: IR: irregular ripeness, W: wilting, SP: superficial pitting and DP: decay presence. A hedonic scale was used to explain the damage level as 0 = absence of damage, 1 = <10%, 2 = 11 – 25%, 3 = 26 – 40% and 4 = >40%. Finally, the following equation was applied (Vega-García et al., 2010):

$$CI = \frac{IR + W + SP + DP}{4} \quad (1)$$

where each symptom had an assigned value as abovementioned.

2.4. Quality parameters

Firmness was determined as the maximum compression force (expressed in N) and performed by the penetration of tomato pericarp sections using a Penetrometer (Chatillon, USA). Total soluble solids (TSS) were measured according to AOAC method 22.014 (AOAC, 2012) using a hand refractometer (Fisher Scientific, Canada) and values were reported as °Brix. For electrolyte leakage (EL), the technique described by López-Velázquez et al. (2020) was used.

2.5. Light microscopy

Portions of tomato tissues (1 cm^3) were obtained from the pericarp equatorial region at days 0, 12 and 12 + 7 (ripening stage) for each temperature (12 and 4 °C), and were placed in FAA fixation for 48 – 72 h. Then, samples were dehydrated throughout six graded ethanol series (50–100%) and later, they were transferred to an absolute ethanol-xylene (1:1). In each solution, samples were immersed for 5 h in stirring (Phothiset & Charoenrein, 2014). After that, samples were included in paraffin blocks to proceed with the obtention of transverse sections of 10 μm by a microtome (Leica, Germany). The samples were then rehydrated in a graded ethanol series (100 to 50%) and differential staining was carried out by using safranin and fast green. Finally, tomato tissue was observed under light microscopy (Zeiss, Germany) using the 10X objective lens.

2.6. Environmental Scanning Electron microscopy (ESEM)

ESEM was performed on tomato fruit stored for 12 days (12 or 4 °C) plus 7 days at 21 °C (12 + 7). The tomato pericarp (mesocarp) and cuticle were cut in areas of 3.5 × 3.5 cm^2 with no previous preparation. Then, trials were observed in an Environmental Scanning Electron Microscope (FEI Quanta, USA) at different magnifications (50 to 1000X), distance work: 10 mm, and a voltage of 2 kV for the secondary electrons detector (LED).

2.7. Atomic force microscopy (AFM)

Tomato cuticle presenting CI and regular ripeness (4 and 12 °C, respectively) at 12 + 7 days were examined in an Atomic Force Microscope (Bruker, USA). For the nanoindentation test, the methodology proposed by Cárdenas-Pérez et al. (2016) was applied. An DNP-10 AFM probe (Bruker, USA) was used with the following features: triangular geometry, nominal tip radius: 20 nm, nominal length: 205 μm, width: 40 μm, thickness: 0.6 μm, nominal frequency: 23 kHz. Also, the calibration of the probe was performed as reported by the previous report and the spring constant (k) was determined in fluid media, resulting in an average k of 0.12 ± 0.01 N/m.

After calibrations, a portion of the tomato was placed between two glass slides (as a sandwich), exposing the cuticle in a gap to be nano-indented (Cárdenas-Pérez et al., 2016). Tests were carried out in "PeakForce" tapping mode using the following conditions: scan size = 5 μm, ramp rate = 1 Hz, force = 50 nN, velocity = 1.5 μm/s, and the area section was 15 × 15 μm^2. A total of 64 points in a regular matrix were analysed. The images were acquired by NanoScope Analysis v1.4 software.

2.8. Digital image analysis

Three scales (micro, micro-nano, and nano) were evaluated to establish a multi-scale descriptive model for the development of CI in tomato tissue. This assessment was based on the performance of digital image analysis in the software ImageJ v.1.50d (National Institutes of Health, USA), which procedure is schematised in Fig. 1.

The micro-scale approach was carried out using images from the light microscopy technique. Briefly, a reconstruction of a larger image (1787 × 2842 $pixels^2$) from individual images was done to have the analysis of the complete tissue. Then, the image processing consisted of a transformation from an RGB image (colour) to an 8-bit image (grey-scale), followed by the threshold selection using an automatic default algorithm to obtain a binary image. Finally, the multifractal behaviour

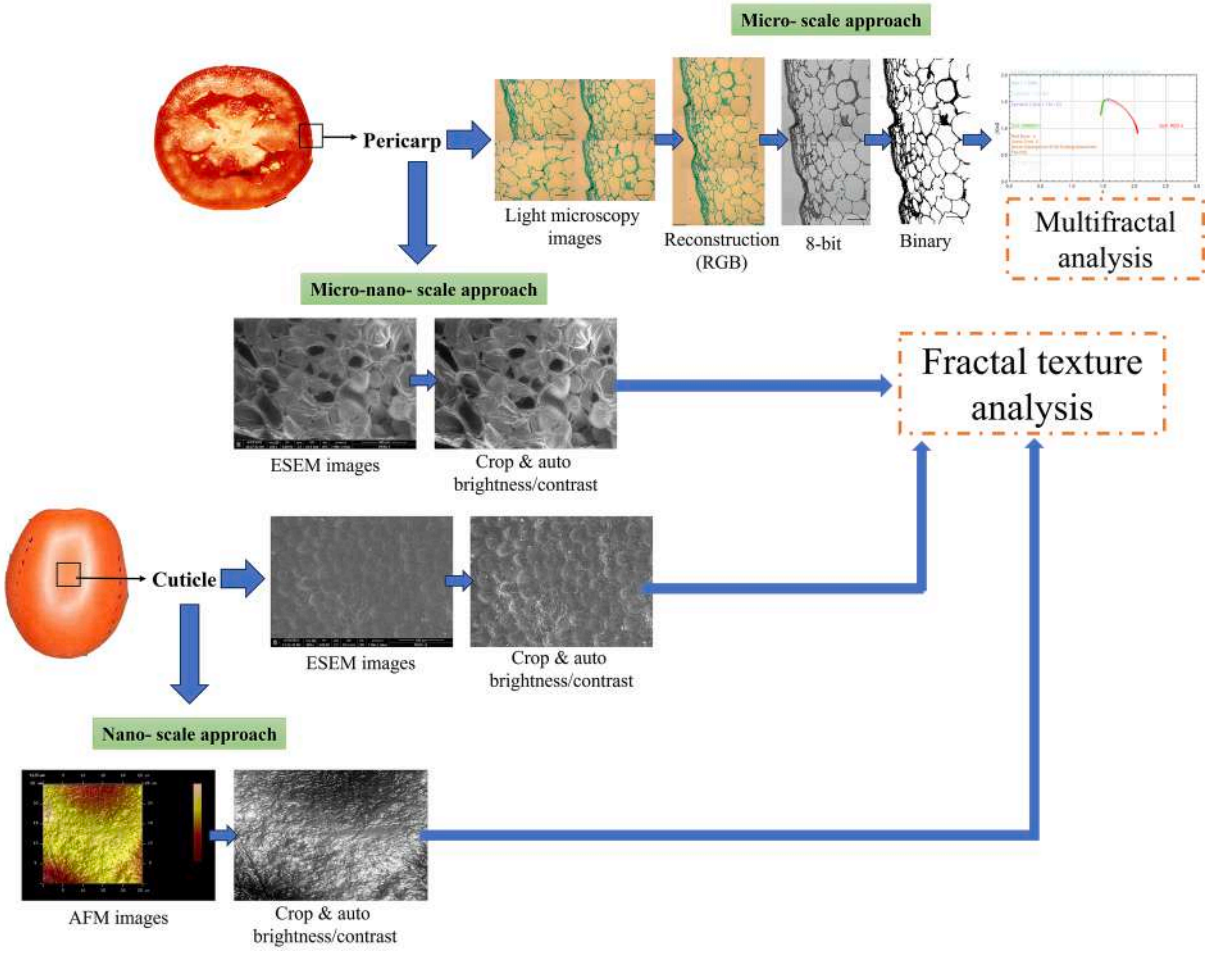

Fig. 1. Scheme of the digital image analysis procedure performed for the multi-scale approach of the CI in tomato tissues.

and lacunarity (Λ) were evaluated with the plugin FracLac 2015Febb5810 for ImageJ software (Cáez Ramírez et al., 2017).

For the micro-nano-scale approach, ESEM images from the pericarp and the cuticle were processed as follows: the RGB image (size: 1536x1103 pixels^2) was cropped (size: 1536x1022 pixels^2), and then, converted into an 8-bit image to proceed with an automatic adjust of brightness and contrast. Finally, FD of texture and lacunarity (Λ) were determined by the plugin FracLac 2015Febb5810. Regarding the nano-scale approach, AFM images from the cuticle were analysed following the same method applied to ESEM images.

2.9. Fractal analysis

The multifractal analysis performed for the micro-scale approach was carried out according to the methodology described by García-Armenta et al. (2014). This method is based on the box-counting method and a multifractal spectrum is obtained to explore different probabilistic regions where a certain fractal dimension can describe the object morphology (da Fonseca de Albuquerque et al., 2022). For q > 0, the generalised fractal dimension (D_q) represents the more singular regions (high probability), and for q < 1, D_q indicates less-singular regions. Also, D_q has been defined as the Hausdorff dimension (Matos et al., 2023). In this sense, $D(q, r_B)$ is the dimensions spectrum for a given data set defined for the following equation (García-Armenta & Gutiérrez-López, 2022):

$$D(q,r) = \frac{1}{q-1}\lim_{r\to 0}\frac{\log\Sigma_{i=1}^{N}[P_i(r)]^q}{\log r_b} \quad (2)$$

where q values are the analysed regions; P_i is the probability to find a certain fractal dimension; r is the observation scale. In this study, $D_{q=0}$, $D_{q=1}$, $D_{q=2}$, corresponding to generalised fractal dimensions for q values of 0, 1 and 2, respectively, were determined. $D_{q=0}$ represents the box-counting fractal dimension with the highest probability to describe the image; $D_{q=1}$ is the entropy dimension which relates the uniformity of all fractal points; and $D_{q=2}$ indicates the correlation dimension between two fractal points (Serrano et al., 2019).

Also, multifractal spectra [$f(a)$ vs α] were obtained for the treatments: 0, 12 and 12 + 7 days at both temperatures (12 and 4 °C). $f(a)$ is the value of the subset of fractal dimensions and α is the singularity of the spectrum.

For the micro-nano- and nano-scale approaches FD and lacunarity (Λ) were determined according to Valenzuela-Lagarda et al. (2018). FD was computed using the following equation (Starodubtseva et al., 2017):

$$FD = \lim_{r\to 0}\frac{\log N_r}{\log\left(\frac{1}{r}\right)} \quad (3)$$

where N is the number of boxes of size r. Also, Λ was calculated as follows (Yaşar & Akgünlü, 2005):

$$\Lambda = \left(\frac{\sigma}{\eta}\right)^2_{r,o} \quad (4)$$

where σ is the mean and η is the standard deviation of pixels per box at a certain size r and orientation, o.

2.10. Statistical analysis

The Fisher test was performed for the comparison of means with a significance level of 95% and was carried out using the Minitab v.17 software (Minitab Inc., USA). Also, Principal Component Analysis (PCA) was applied to a standardised data set (firmness, TSS, EL, D_q, FD, Λ) based on 20 tomato samples for each temperature (12 and 4 °C) in the Origin 2019b software (OriginLab, USA).

3. Results and discussion

3.1. CI index

Values of the CI index in tomatoes stored for 12 days at 4 °C and 12 + 7 days at 21 °C were significantly different ($p \leq 0.05$) to unripe tomatoes (day 0) indicating that these products presented typical symptoms of CI such as irregular ripeness, abnormal softening, and necrosis, that intensified during ripening (Fig. 2A). In this sense, it has been reported that these symptoms are a result of metabolic changes, the production of reactive oxygen species, and changes in lycopene synthesis (Loayza et al., 2021). While the fruit stored at 12 °C for 12 days, did not present significant differences ($p > 0.05$) as compared to unripe tomatoes (day 0) due to 12 °C is a safe temperature for tomato storage. These samples exhibited regular ripeness, an intense and bright red colour without apparent damage, which were common fruit features.

3.2. CI evaluation by quality parameters

One of the most important parameters for evaluating fruit quality is firmness. A significant reduction ($p \leq 0.05$) of 29% in tomato firmness was observed after 12 days at 12 °C (safe temperature) in comparison to the initial conditions (day 0). After the ripening stage, firmness was significantly reduced ($p \leq 0.05$) by 50% as compared to day 12 (Fig. 2B). This behaviour was associated with regular changes belonging to the ripening process (Tilahun et al., 2019). On the other hand, fruit stored at CI temperature maintained the firmness after 12 days, but during ripening conditions (12 + 7 days) tomatoes presented a 46% firmness reduction in comparison to day 12. This loss of firmness in tomatoes was probably caused by the enhanced pectin solubility present in the cell wall which resulted in higher enzymatic activities of pectin methylesterase and polygalacturonase (Carvajal et al., 2015). In addition, Biswas et al. (2012) reported that regular-ripe tomatoes exhibited lower firmness values in comparison to chilled fruit (stored at 6 °C for 27 days and transfer to 20 °C), indicating that a common symptom of CI is the irregular ripeness.

Also, TSS is one of the most evaluated fruit quality parameters and indicates the ratio of intracellular solutes in the fruit. In this sense, significant differences ($p \leq 0.05$) were found in TSS values for all trials stored at 12 °C (Fig. 2C), exhibiting significant TSS increments throughout the storage days. It is well known that TSS values rise during the typical ripening process due to starch being degraded into sugars by the enzymatic activity carried out throughout metabolic pathways (Adi et al., 2019; Wang et al., 2021). Conversely, at 4 °C, a significant increase ($p \leq 0.05$) in the TSS was observed between days 0 and 12, and after that, a significant decrease was identified at the ripening stage (12 + 7 days). This increment can be associated with the accumulation of sugars as a protective mechanism (Zhang et al., 2019); whilst, the TSS reduction in tomatoes with CI was probably due to the use of sugars as an energy source to avoid stress (Rasouli et al., 2019).

Furthermore, another index that reveals CI is EL, which is an

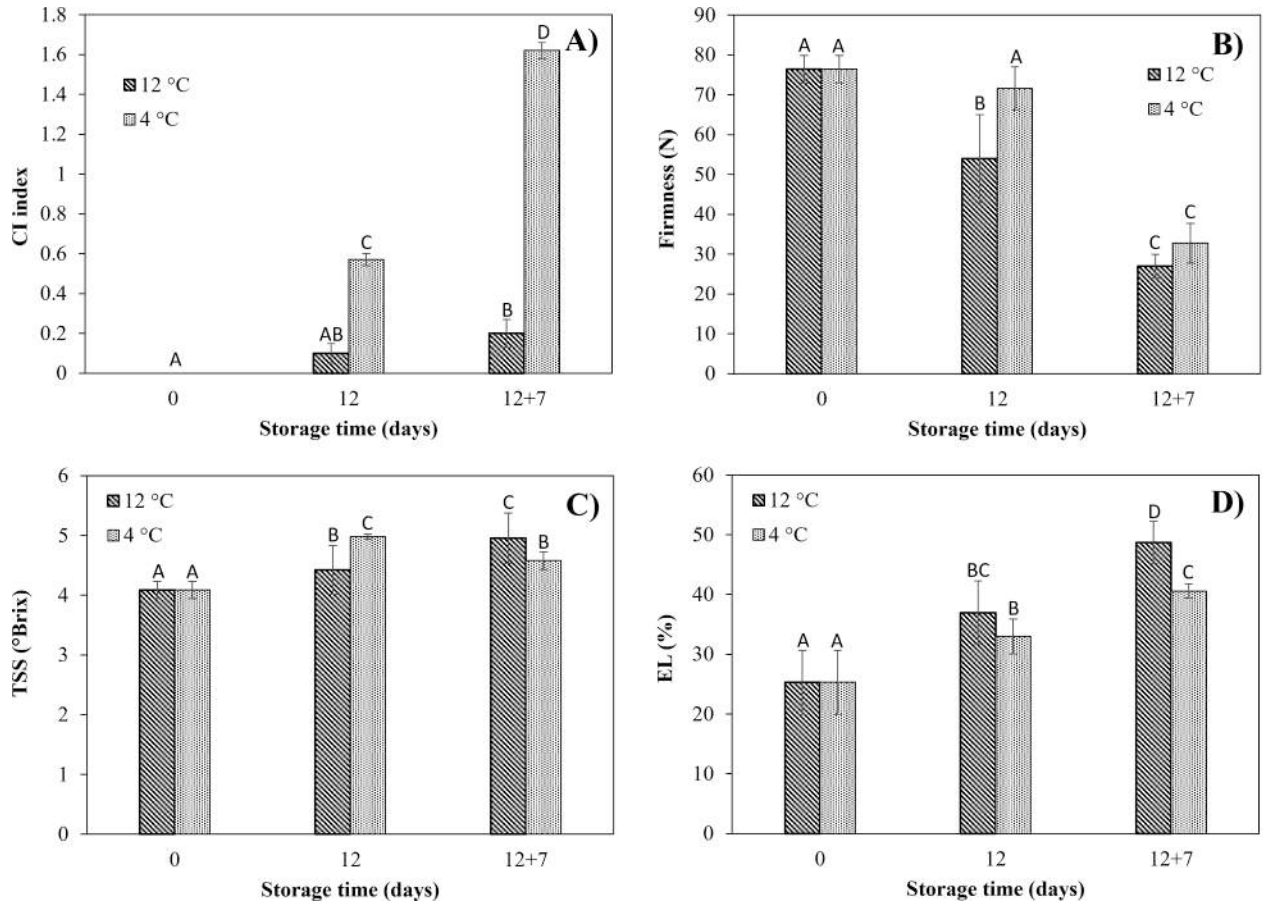

Fig. 2. A) Chilling injury (CI) index, B) firmness, C) total soluble solids (TSS) and D) electrolyte leakage (EL) of tomato at different storage days and temperatures. Different capital letters indicate significant differences ($p \leq 0.05$) between pairs of means by Fisher's test.

indicator of integrity loss in the plasma membrane. EL values of all treatments for both temperatures (12 and 4 °C) were significantly different ($p \leq 0.05$) as compared to day 0 (taken as a control for statistic tests) (Fig. 2D). Particularly, 12 °C stored tomatoes at the ripening stage (12 + 7) possessed the highest EL values compared to day 12 due to the increased membrane permeability in a typical ripening process. Similarly, higher EL values were observed for tomatoes with CI (day 12 + 7) compared to day 12. This may be related to the fact, that in healthy temperatures the symptoms of CI intensify. In this sense, it is well known that CI increase EL values during the ripening stage of several agricultural products (Liu et al., 2019; Pan et al., 2019; Venkatachalam, 2018).

3.3. Micro-scale evaluation of CI

Fig. 3 depicts tomato tissue during storage at different temperatures. At day 0, a homogeneous structure was observed, exposing mesocarp cells having ovoid shapes. In tomatoes stored at 12 °C, a typical ripening process was detected owing to tissues with regular cell shapes and sizes.

Most of the histological changes in tomatoes were exhibited in samples stored at 4 °C in which the integrity of mesocarp cells was affected since day 12, observing different cell shapes, as well as more compacted cells towards the cuticle during the ripening stage (12 + 7 days). Besides, at this stage, the cuticle and the exocarp had more irregular shapes possessing a wave pattern. A deeper histological comparison between healthy and damaged tissue can be found in Supplementary material (Section b.1). Carvajal et al. (2015) studied CI in zucchini, finding that at a microscopic level, collapsed cells were identified in damaged samples which can be attributed to cell wall solubilisation and depolymerisation. Therefore, CI can be detected early using the monitoring of light microscopy images due to visual differences were evident. However, the CI evaluation based on visual features represents a subjective approach and standardised and mathematical tools such as fractal analysis are needed to achieve an enhanced micro-scale approach to this physiological disorder.

3.3.1. Multifractal analysis

The multifractal approach was suitable to quantitatively describe the morphometric behaviour of tomato tissue during CI based on images acquired by light microscopy. The multifractal evaluation was decomposed in tangled fractal sets which were characterised by $f(\alpha)$, i.e., the fractal dimension of the boxes set and their singularity strength (α) (García-Armenta & Gutiérrez-López, 2022). In this sense, the plot (i.e., multifractal spectrum): $f(\alpha)$ vs. α allowed distinguishing the distribution of the space filled by the tomato tissue and thus, explaining its irregularity. Fig. 4 shows multifractal spectra corresponding to tomato tissues subjected to all treatments. A space between all the analysed sets was observed, which is characteristic of multifractal patterns and reflects the strength of the multifractal nature assumed by the object (Matos et al., 2023). This space is called the "arms" of the multifractal spectrum and its width has been related to the probability of having a certain multifractal behaviour to describe a certain object (Ţălu et al., 2015). Particularly, when a figure is mono-fractally distributed, α is identical in all regions (q values), hence the multifractal spectrum consists of a single point; therefore, α (or the width spectrum) indicates the degree of the image heterogeneity (Serrano et al., 2013). Also, the plots were built for q values from −10 to 10 and generalised fractal dimensions (D_q) were obtained for q = 0, q = 1 and q = 2. All multifractal spectra revealed similar shapes; however, they could be differentiated by their D_q values. Table 1 shows the extracted multifractal parameters, indicating a general tendency for all treatments of $D_{q=0} > D_{q=1} > D_{q=2}$, which confirmed the multiscaling behaviour by the representation of a decreasing function among the complexity parameters and denoting differences among microstructure patterns (Jung & Yoon, 2017). In this case, no significant differences ($p > 0.05$) were found for $D_{q=1}$ and $D_{q=2}$ values as compared the trials at day 0, day 12 (for both temperatures) and day 12 + 7 at 12 °C (Table 1). Nevertheless, these generalised fractal dimensions were significantly different ($p \leq 0.05$) at chilling conditions (day 12 + 7, stored at 4 °C) in comparison to the rest of the treatments (Table 1), demonstrating that chilled tissues were damaged producing morpho-structural variations in terms of uniformity and pattern complexity. In this sense, most of the changes were detected by $D_{q=0}$ values (generalised fractal dimensions at the peak of each graph), which varied between 1.57 and 1.66 (Table 1). The results indicated that the

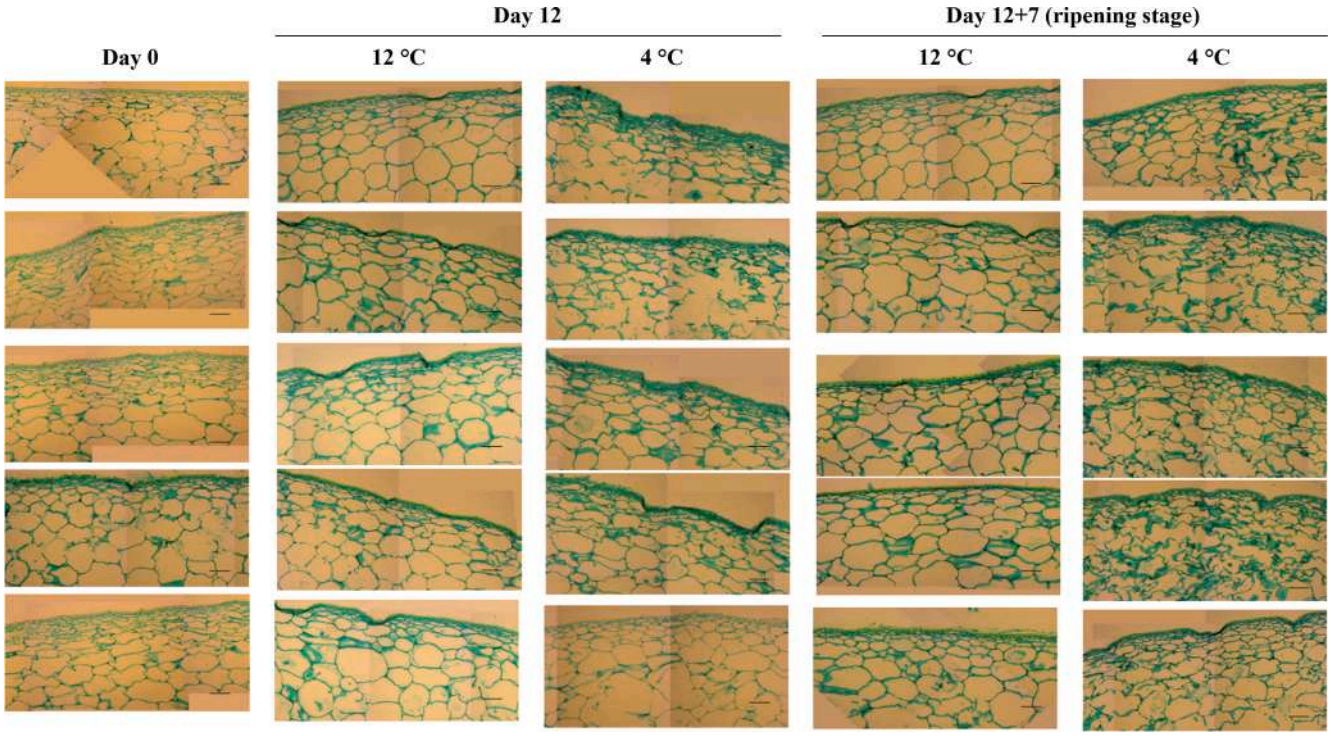

Fig. 3. Reconstructions of light microscopy images of five different tomato samples for different storage days at 12 °C and 4 °C. The scale bar represents 2 mm.

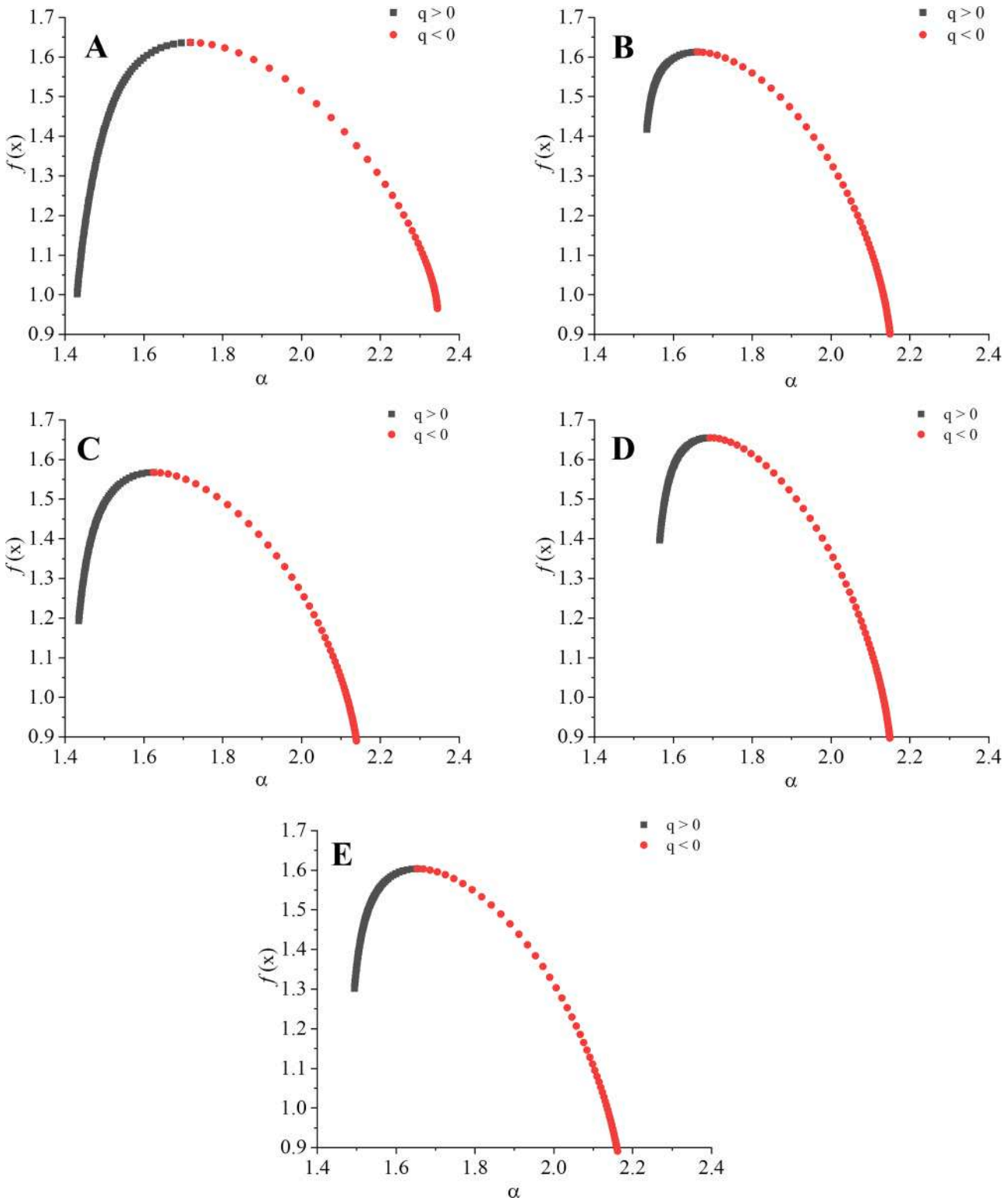

Fig. 4. Multifractal spectra [$f(a)$ vs α] of light microscopy images of tomato tissue stored at A) 0 days; B) 12 days at 12 °C; C) 12 days at 12 °C plus 7 days at 21 °C (12 + 7: ripening stage with no chilling injury); D) 12 days at 4 °C; E) 12 days at 4 °C plus 7 days at 21 °C (12 + 7: ripening stage with chilling injury).

multifractal spectrum corresponding to the tomato tissue at day 0 (without storing) was wider (Fig. 4A) having a lower $D_{q=0}$ value ($p \leq 0.05$) (Table 1) in comparison to the tissue at storage conditions of 12 days at 12 °C (Fig. 4B). During the storage period at 12 °C, delayed metabolic pathways associated with ripening occur in tomatoes producing less irregular cell tissue but possessing a higher heterogeneity at this stage. Subsequently, a significant increase ($p \leq 0.05$) of the $D_{q=0}$ value was observed for tomato tissue stored for 12 days at 12 °C plus ripening period (12 + 7) as compared to the previous stage (12 days) at the same temperature (Table 1). However, no differences were detected in widths of the multifractal spectra of day 12 and 12 + 7 at 12 °C (Fig. 4C). This finding can be related to a more irregular tomato tissue

Table 1
Multifractal parameters of tomato tissues at different storage days and temperatures.

	Storage time (days)		
	0	**12**	**12 + 7 (ripening stage)**
Temperature (°C)	$D_{q=0}$		
12	1.630 ± 0.026^{A}	1.579 ± 0.012^{D}	1.606 ± 0.002^{B}
4	1.630 ± 0.026^{A}	1.624 ± 0.015^{AB}	1.659 ± 0.006^{C}
	$D_{q=1}$		
12	1.616 ± 0.032^{A}	1.600 ± 0.021^{A}	1.605 ± 0.017^{A}
4	1.616 ± 0.032^{A}	1.612 ± 0.029^{A}	1.646 ± 0.022^{B}
	$D_{q=2}$		
12	1.606 ± 0.029^{A}	1.588 ± 0.021^{A}	1.591 ± 0.018^{A}
4	1.606 ± 0.029^{A}	1.602 ± 0.028^{A}	1.630 ± 0.022^{B}
	Λ		
12	0.3027 ± 0.025^{AB}	0.3809 ± 0.026^{C}	0.3394 ± 0.034^{AB}
4	0.3027 ± 0.025^{AB}	0.3390 ± 0.044^{BC}	0.2933 ± 0.033^{B}

D_q: generalised fractal dimension at $q = 0$, $q = 1$, and $q = 2$; Λ: lacunarity. Different capital letters indicate significant differences ($p < 0.05$) between pairs of means by Fisher test.

(higher fractal dimension), maintaining a similar cell heterogeneity, due to high respiration rates during a regular ripening process. Also, this tissue irregularity agreed with the loss of firmness and increased EL detected at day 12 + 7 (see Section 3.2). In this sense, increased fractal dimensions have been found in ripe papayas (85% vs. 65% ripe), assigning this behaviour to a heterogeneous decrease in colour parameters, enhanced respiration rates and the ethylene action (Cáez Ramírez et al., 2017).

Regarding tomatoes exposed at 4 °C, $D_{q=0}$ values were not significantly different ($p > 0.05$) between days 0 and 12 (Table 1) as well as no differences were found in tomato firmness during this storage period (see Section 3.1). Analogously, similar widths were observed in multifractal spectra corresponding to days 0 and 12 (Fig. 4D). Therefore, the morphology and heterogeneity of cells were not affected by 4 °C conditions at this postharvest stage period (day 12). However, tomato tissue with CI symptoms (storage day: 12 + 7, ripening stage) had the highest $D_{q=0}$ value ($p \leq 0.05$) and the lowest width of the multifractal spectrum as compared to the rest of the treatments. This result meant that damaged cells by cold storage were irregular, and this irregularity was heterogeneous throughout the tissue image.

Besides the fractal dimension, lacunarity (Λ) is a parameter that completes the fractal description of a figure. Λ of an image describes its homogeneity (based on the distribution of pixels) and symmetry using the measurement of gaps (or "lacunae") in a digital image (García-Armenta et al., 2019). Objects with similar fractal dimension values can be symmetrically differentiated by a distinct Λ value due to their self-similarity does not fill the measuring box (in the box-counting method) at the same ratio. Hence, a high Λ value has been related to a less symmetric image (García-Armenta et al., 2021). For tomato tissue stored at 12 °C, a significant increase ($p \leq 0.05$) of Λ was observed for storage day 12 in comparison to day 0, which was associated with a higher proportion of gaps in the images. The regular ripening of tomatoes causes an increase in the structural separation of cells resulting in firmness loss and a higher tissue asymmetry. When 12 °C stored tomatoes were subjected to ripening conditions (day 12 + 7), the Λ value significantly decreased ($p \leq 0.05$) probably due to common structural changes at the ripening stage that organised the tissue in a more symmetric figure.

On the other hand, significant differences ($p \leq 0.05$) in Λ values were found only between day 0 and the ripening stage (12 + 7) under CI conditions, demonstrating that the irregularity described by $D_{q=0}$ in CI tissues was symmetric along the images. Comparing the Λ of all treatments against day 0, stored tomatoes for 12 days at 12 °C possessed the highest value, indicating that at a micro-scale level of observation, structural damage can be identified in cells and possibly this injury was not detectable at a macro-scale level (visual examination). The CI evaluation by fractal parameters has been scarcely studied; however, Espinosa-Velázquez et al. (2016) evaluated the morphology during the ripening of avocados through the light microscopy technique, finding that Λ was higher in unripe avocados in comparison to ripe trials, i.e., the ripening stage triggers more symmetrical fruit tissues.

The abovementioned results indicated that morphological changes of tomato tissues affected by CI can be successfully described by the multifractal approach at a micro-scale level observation.

3.4. Micro-nano-scale evaluation of CI

ESEM technique allows to detect changes at a micro-nano-observation scale level (García-Armenta & Gutiérrez-López, 2022). Based on the findings determined by the micro-scale level, changes in tomatoes caused by CI were mainly distinguishable at the ripening stage (12 + 7) (See Fig. 3). Therefore, ESEM images were acquired during this period to focus on structural changes carried out only by this disorder.

Regarding the visual evaluation of ESEM images of tomato pericarp at the ripening stage (12 + 7), fruit stored under 12 °C conditions presented cells with regular shapes, intact cell walls and no visible damaged tissue when observed at 50X (Fig. 5A) and 100X (Fig. 5C). Conversely, those previously stored at 4 °C (with CI) exhibited alterations in cells such as more elongated cells and broken cell walls (Fig. 5B and 5D). Besides, ESEM images revealed that CI in tomatoes triggered a significant increase ($p \leq 0.05$, by Tukey test) in cell size (mean = 235.7 ± 89.4 μm) in comparison to regular ripe fruit (mean = 130.22 ± 53.89 μm) and a different cell size distribution. The methodology to achieve these data can be found in Supplementary material (Section a.1). Fig. 5E shows cell size distribution for both storage temperatures (12 and 4 °C), determining that the size distribution corresponding to cells of non-chilled tomatoes possessed a Log-normal distribution type ($p = 0.533$, by Anderson-Darling test) skewed to the left (skewness = 1.165; kurtosis = 1.306); whilst, cells with CI resulted in a symmetrical (skewness = 0.225; kurtosis = -0.993) 3-parameter Weibull distribution type ($p = 0.138$, by Anderson-Darling test). In this sense, the micro-nano-observation scale level of CI damage has been studied for mangoes using X-ray μCT technique, finding that the pore size (produced by cell networks in 3D) of healthy mesocarp was lower in comparison to the mesocarp developing CI, which presented pore collapse and an increased pore space among cells (Cantre et al., 2017).

Regarding the tomato cuticle observed by ESEM, that corresponding to ripe fruit stored at 12 °C exhibited a more uniform texture and their shapes were more regular in comparison to tomatoes stored at 4 °C (CI condition) (Fig. 5F and 5G). Irregular ripening is one of the most common CI symptoms, and ESEM images allowed the detection of differences in the grayscale level pixels of the surface belonging to damaged tomato cuticle. Damage was identified as lighter spots in the ESEM images at both magnifications: 250X and 1000X (Fig. 5H and 5I). As previously reported in tomato fruit, the exposition to chilling stress lead to a down-regulation of genes involved in carotenoid synthesis, which could explain the differences in grayscale levels between tomato cuticle stored at 12 and 4 °C (Cruz-Mendívil et al., 2015).

Concerning the fractal analysis, ESEM images were analysed under the multifractal approach which was unsuitable for CI evaluation in tomatoes due to the α distribution resulted in a single point (data not shown). Therefore, the monofractal dimension (FD) of texture based on pericarp and cuticle images was calculated for all treatments. FD is a morphometric parameter that has been associated with the irregularity and rugosity of a surface (Valenzuela-Lagarda et al., 2018). Results indicated that both FD values from the pericarp and the cuticle were significantly higher ($p \leq 0.05$) at the CI conditions (Table 2) which could be associated with more irregular and rougher surfaces in several zones of the tomato tissue. However, no significant differences ($p > 0.05$) were

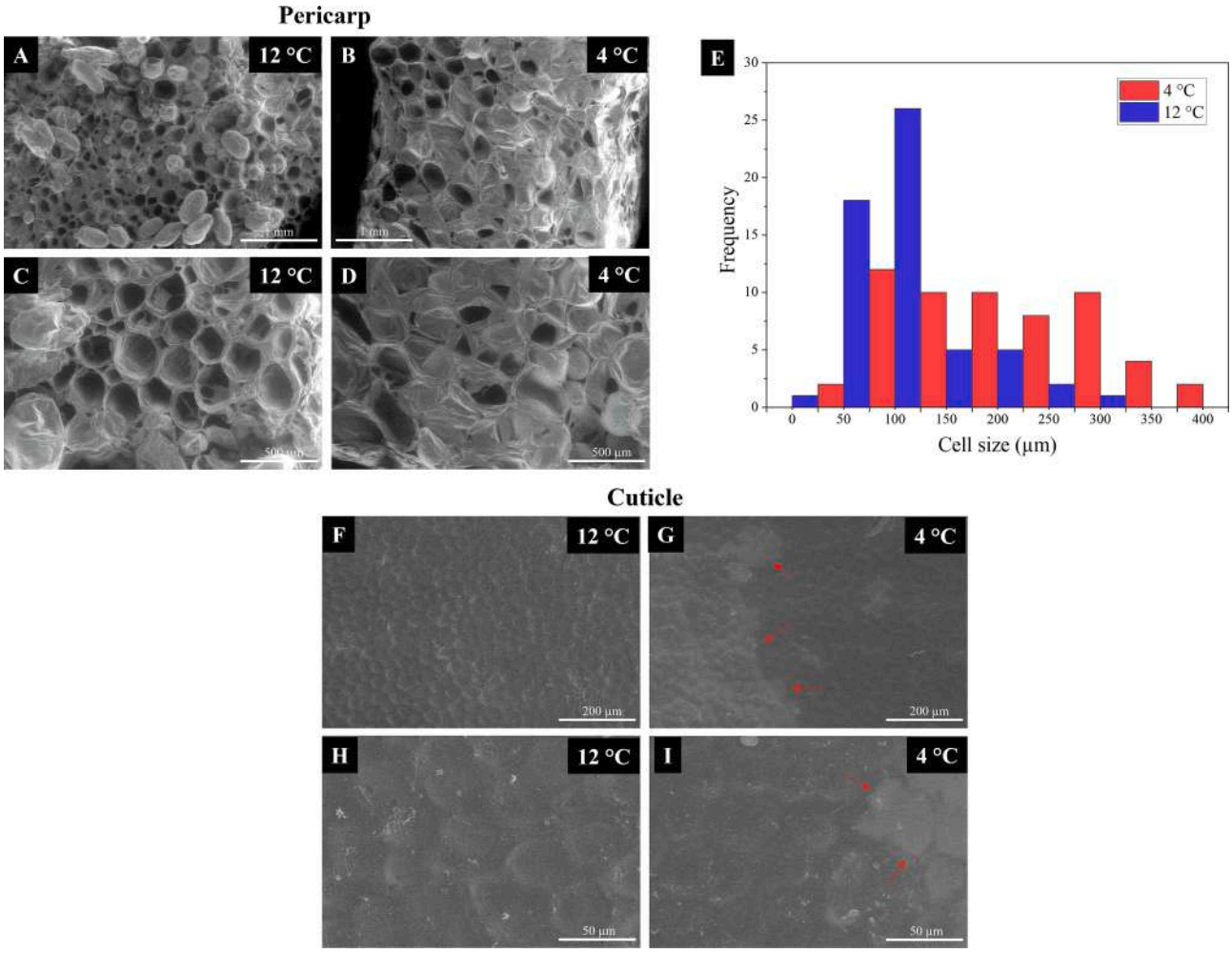

Fig. 5. ESEM images of the pericarp and cuticle of tomato taken after 12 days of storage at 12 or 4 °C plus 7 days at 21 °C, at magnifications of 50X (A and B), 100X (C and D), 250X (F and G), 1000X (H and I). E) Cell size distribution of tomato tissues with (4 °C) and without (12 °C) chilling injury (CI). Red arrows indicate lighter surfaces.

Table 2
Morphometric parameters of tomato at ripening stage (12 storage days plus 7 days at 21 °C) from ESEM and AFM images.

Parameter	Storage temperature (°C)	
	12	4
ESEM		
FD_p	1.578 ± 0.009^{B}	1.601 ± 0.013^{A}
Λ_p	0.031 ± 0.008^{A}	0.0472 ± 0.031^{A}
FD_c	1.644 ± 0.031^{B}	1.746 ± 0.048^{A}
Λ_c	0.029 ± 0.015^{A}	0.014 ± 0.022^{A}
AFM		
FD	1.609 ± 0.045^{A}	1.626 ± 0.027^{A}
Λ	0.044 ± 0.038^{A}	0.025 ± 0.009^{B}
R_a(nm)	157.0 ± 51.2^{B}	231.9 ± 70.4^{A}
R_q(nm)	199.9 ± 56.3^{B}	288.9 ± 84.7^{A}

FD: fractal dimensión; Λ: lacunarity; R_a: arithmetic rougness; R_q: root mean square roughness.
Subscript *p* means pericarp and subscript *c* means cuticle.
*Different capital letters indicate significant differences ($p \leq 0.05$) among means by Fisher test.

found for Λ values between ripe tomatoes at 12 and 4 °C. These findings meant that the texture irregularity detected by FD was uniformly distributed in the entire image, given that Λ is a parameter that associates the figure geometry and the texture quality (Matos et al., 2021). There have been some reports using Scanning Electron Microscopy (SEM) technique for the description of CI in different fruit such as bananas (Huang et al., 2021), blood oranges (Habibi et al., 2020), and green bell peppers (Kong et al., 2020). However, FD has not been considered a parameter to detect CI symptoms at the micro-nano-scale observation level. Based on this study, FD can be an appropriate indicator of cell damage induced by CI in tomato fruit.

3.5. Nano-scale evaluation of CI

AFM technique involves the use of nanoindentation to obtain detailed images of the surface of a certain object at the nano-scale level of observation. In this study, AFM images were acquired to assess CI in tomato cuticle. The observation of the tomato nanostructure revealed that wax was present in all samples. For non-chilling conditions (tomatoes stored at 12 °C), wax was responsible for the creation of smoothed lines in the images (Fig. 6A and 6B); whilst the wax in CI tissue (tomatoes stored at 4 °C) formed small edges or bumps at the cuticle surface (Fig. 6C and 6D). It is important to mention that substantial changes in this element (wax) were unable to detect at micro- and micro-nano-scale level observations which were described in previous sections. Also, in AFM images, darker zones (dark red colour) corresponded to deeper regions and lighter zones (yellow colour) are shallower areas. Therefore, results showed that CI nano-scale level produced rougher

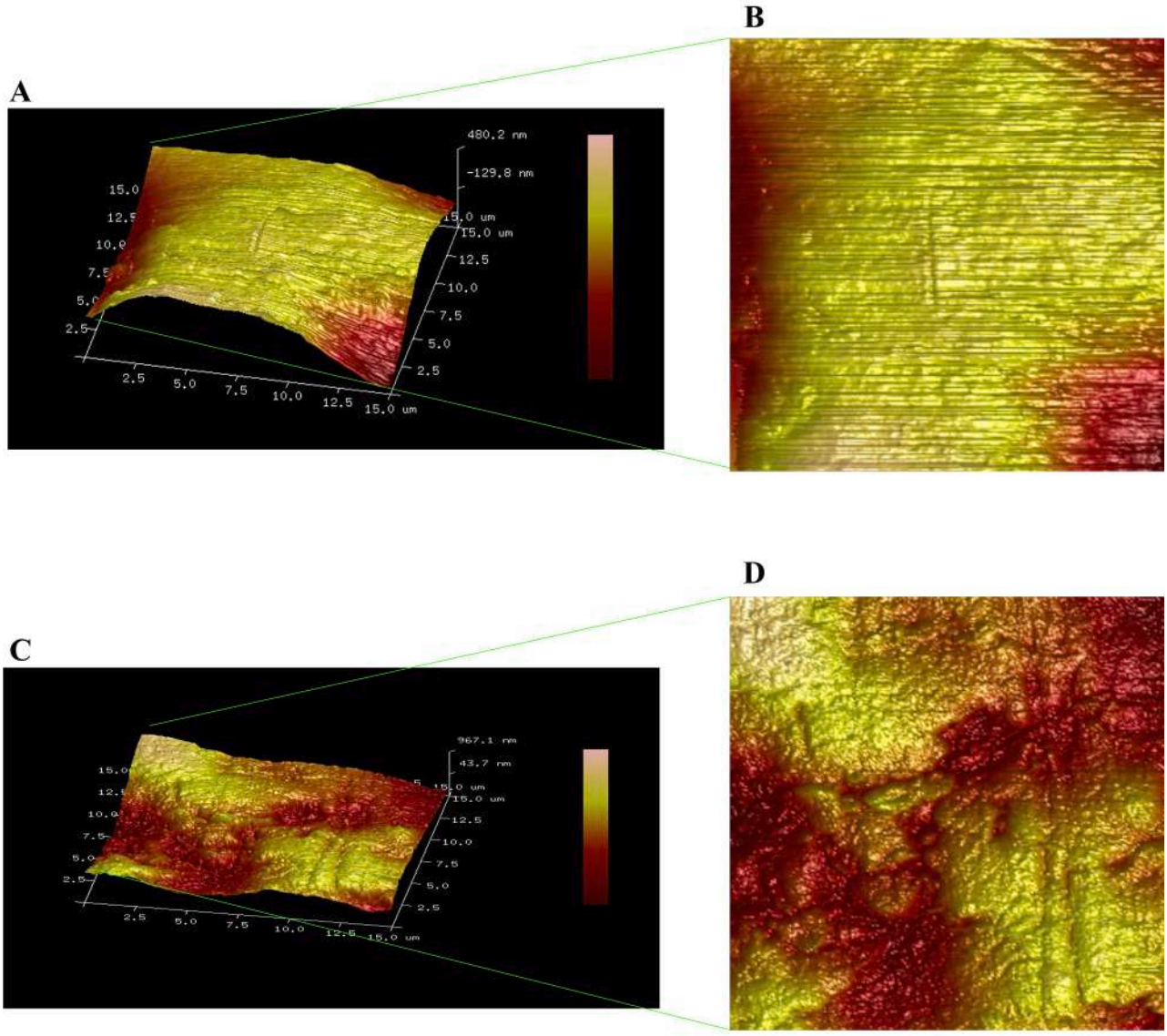

Fig. 6. AFM images in an area of 15 × 15 μm^2 of tomato cuticle at the ripening stage (12 storage days plus 7 days at 21 °C) when tomato was stored at 12 °C, non-CI conditions (A and B) and 4 °C, CI conditions (C and D). Left images represent 3D plots and right images are their corresponding 2D view.

areas in comparison to non-chilled tissue (See Fig. 6). It was remarkable that a related result was detected at the micro-scale approach due to the CI tissue possessed more deformations and non-chilled samples exhibited smoother structures (see Fig. 3). In this sense, the AFM technique has been successfully applied to fresh vegetable tissues. Li et al. (2011) reported similar findings, indicating that CI in sweet peppers triggered AFM signals which depicted bumps and rough surfaces in the epicarp of these products.

Based on the visual evaluation of the AFM images, it was clear that there were morphological differences between healthy and CI tomato tissue at the nano-scale approach. However, FD values calculated from AFM images did not show significant differences ($p > 0.05$) (Table 2) between both temperatures, indicating that this parameter was inadequate to detect changes in the nanostructure of tomato tissue damaged by CI. It is well known that FD is strongly dependent of the observation scale; hence, this parameter worked well for micro- and micro-nano-approaches but not for the nano-scale.

Conversely, significant differences ($p \leq 0.05$) were found in Λ (Table 2), detecting lower values for CI conditions as compared to regular ripe samples, which meant that the images corresponding to injured tissues were more symmetrical in comparison to non-damaged fruit. In a study, the fractal analysis based on AFM images was helpful to distinguish apple tissues and isolated cells at a nanometric scale, reporting that FD was higher in isolated cells than in tissues (Cárdenas-Pérez et al., 2016).

On the other hand, the roughness extracted from AFM images as R_a and R_q parameters was assessed to couple the fractal analysis. Higher values of both parameters indicate higher heights of the analysed surface. Data showed that the roughness belonging to CI tomato samples was significantly higher ($p \leq 0.05$) than non-chilled tissue (Table 2), which could be associated with the bumps observed for cell damage caused by the exposition to chilled temperatures. Consequently, R_a and R_q resulted in suitable parameters to identify CI symptoms at a nano-scale level observation. Khodabakhshian and Baghbani (2021) obtained roughness parameters from AFM images of banana peel to evaluate the ripeness degree, finding that R_a and R_q values decreased (R_a = 8.25–1.12 nm; R_q = 9.65–1.12 nm) in advanced ripening stages. Therefore, roughness parameters could help detect changes that a visual inspection would not achieve concerning the fruit nanostructure during postharvest.

3.6. Principal component analysis (PCA)

In this study, PCA was applied to evaluate interactions between quality and morphometric parameters (at analysed observation scales) as they were affected by the CI in tomato (Fig. 7). This analysis suggests that factors can be included in a first component (PC1) if they have a high relationship among them, and the second highest variance value can be supported by a second component (PC2) (Ahmadian-Kouchaksaraie et al., 2016). Results showed that PC1 and PC2 explained the 46.97% of the cumulative data variance. The eigenvalues of the four main components are described in Supplementary material (Table S1).

It can be observed that FDE (fractal dimension from ESEM images), TSS and EL were highly related to positive values of PC1, and their higher values were directed to most chilled samples. This finding meant that a strong interaction was detected for these parameters at chilling conditions. Also, FDA (fractal dimension from AFM images) was related to another cluster of CI tomatoes; however, no interactions with quality parameters were identified. On the other hand, Firm (firmness), $D_{q=0}$ (box-counting fractal dimension), LacA (lacunarity from AFM images) and LacE (lacunarity from ESEM images) were the parameters with the lowest interactions according to PCA. Based on these results, it can be inferred that fractal dimension (at micro and micro-nano-scales) coupled with TSS and EL were the most useful factors to describe morphometric changes yielded by the CI in tomato. Therefore, a descriptive model of this phenomenon must be proposed to improve the understanding of CI and to develop novel technologies for its detection in tomatoes.

3.7. Multi-scale approach

A descriptive model of the changes occurred in tomato tissue by CI was proposed to highlight the dependence of the observation scale in the monitoring of this phenomenon (Fig. 8). FD was a suitable index for the identification of CI symptoms at micro- and micro-nano-levels, suggesting that tissue was more irregular (higher FD values) at chilling conditions. However, this parameter did not detect cell damage at a nano-observation scale; hence, Λ and roughness helped distinguish variations in cell tissues at this level. At nano-observation scale, the cell surface showed alterations produced by CI, exhibiting rougher (higher R_a and R_q) nano areas but symmetrically distributed (lower Λ) into the analysed section. This multi-scale approach could aid to identify cell damage at different observation scales that are not easily detected by subjective visual evaluation (macro level). Also, CI has been scarcely studied by a multi-scale perspective, hence, this study involves several observation scales to propose further techniques to avoid this physiological disorder in postharvest technology.

4. Conclusions

Morphometric changes induced by CI in tomato tissue were described based on the fractal analysis at three observation scales: micro-, micro-nano- and nano-. The light microscopy images revealed that tomato tissue was characterised better by a multifractal behaviour, which meant several fractal dimensions could explain the irregularities observed. Besides, the micro-nano-approach was established by ESEM images, and the nano-observation scale was performed by analysing AFM images. In general, FD (seen as $D_{q=0}$, as well) values (>1.6) were higher for samples presenting CI at the micro and micro-nano-approaches in comparison to non-chilled tissue (FD > 1.5). Additionally, FD can be considered a proper indicator of CI due to it being well correlated with TSS and EL according to PCA. On the other hand, Λ was useful to detect variations only at the nanometric observation scale, finding no differences for the rest of the scales. Also, at the nano-scale approach, roughness parameters (R_a and R_q) completed the identification of changes produced by CI in tomatoes because of higher values were observed for trials at chilling conditions. The suggested multi-scale approach could improve the understanding of CI as a complex disorder which affects the structure of tomato tissues at different observation scales. By the comprehension of morphometric changes carried out in tomato tissues as a consequence of CI, novel methods that act directly on

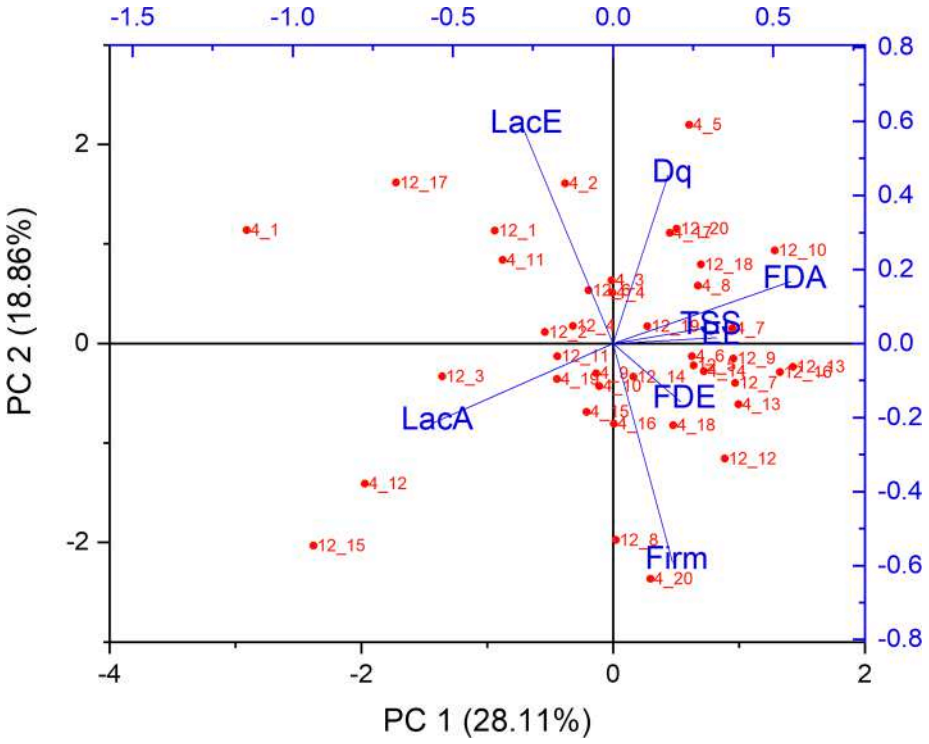

Fig. 7. Principal Component Analysis (PCA) of quality and morphometric parameters. Sample code: storage temperature_sample number. Abbreviations: Firm: firmness; TSS: total soluble solids; EL: electrolyte leakage; Dq: generalised fractal dimension from microscopy images; FDE: fractal dimension from ESEM images; FDA: fractal dimension from AFM images; LacE: lacunarity from ESEM images; LacA: lacunarity from AFM images.

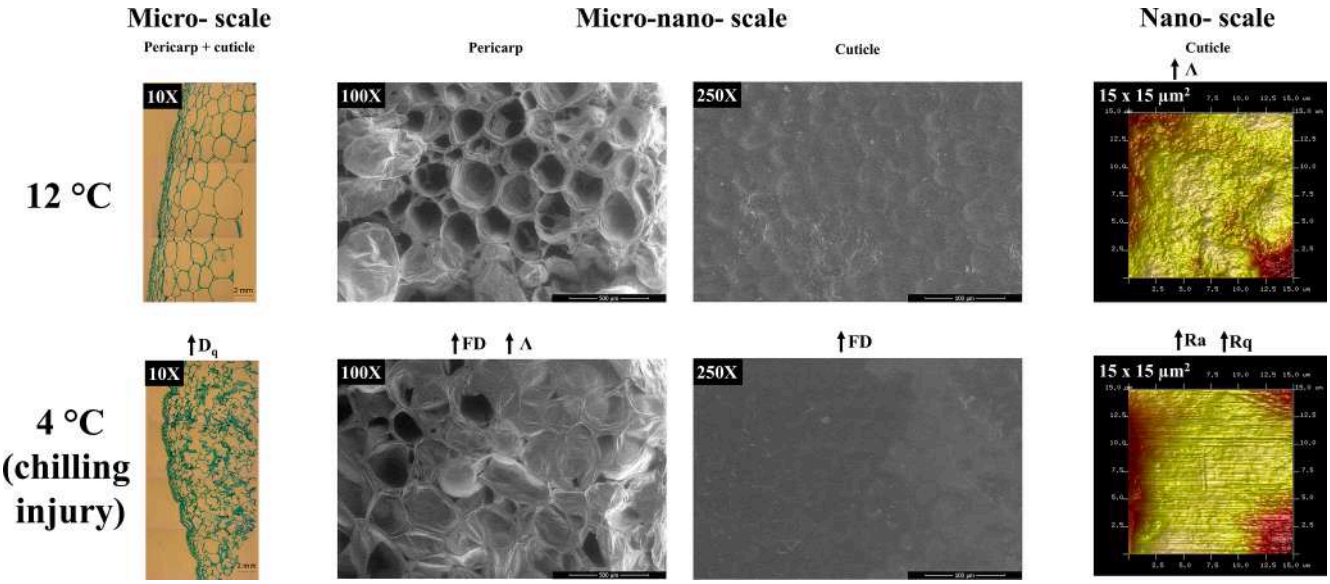

Fig. 8. A Multi-scale descriptive model of morphometric changes derived from chilling injury in tomato. The morphometric parameters placed on top of the photo are the result of the comparison between non-chilling conditions (12 °C) and chilling injury (4 °C). Symbol: ↑ indicates higher values.

cells at each scale can be developed to avoid this postharvest issue.

CRediT authorship contribution statement

C.I. Acosta-Ramírez: Methodology, Software, Investigation, Data curation. **I.D. Lares-Carrillo:** Methodology, Software, Investigation, Data curation. **L.E. Ayón-Reyna:** Formal analysis, Writing – original draft, Writing – review & editing, Visualization, Supervision. **M.E. López-López:** Formal analysis, Writing – original draft, Writing – review & editing, Visualization. **M.O. Vega-García:** Resources, Writing – review & editing. **J.G. López-Velázquez:** Formal analysis, Writing – original draft, Writing – review & editing. **G.F. Gutiérrez-López:** Resources, Writing – review & editing. **U. Osuna-Martínez:** Resources, Writing – review & editing. **E. García-Armenta:** Conceptualization, Formal analysis, Funding acquisition, Project administration, Supervision, Visualization, Writing – original draft, Writing – review & editing.

Declaration of Competing Interest

The authors declare that they have no known competing financial interests or personal relationships that could have appeared to influence the work reported in this paper.

Data availability

Data will be made available on request.

Acknowledgements

This work was supported by Universidad Autónoma de Sinaloa under funding PROFAPI 2022 (PRO_A7_016). Authors Acosta-Ramírez and García-Armenta thank IBQ M. Rosario Galindo-Atienzo, Dr. J. Marcial Zazueta-Moreno and Dr. J. Guadalupe Rendón-Maldonado for the technical support.

Appendix A. Supplementary material

Supplementary data to this article can be found online at https://doi.org/10.1016/j.foodres.2023.113822.

References

Adi, D. D., Oduro, I. N., & Tortoe, C. (2019). Physicochemical changes in plantain during normal storage ripening. *Scientific African, 6*, e00164.

Ahmadian-Kouchaksaraie, Z., Niazmand, R., & Najafi, M. N. (2016). Optimization of the subcritical water extraction of phenolic antioxidants from Crocus sativus petals of saffron industry residues: Box-Behnken design and principal component analysis. *Innovative Food Science & Emerging Technologies, 36*, 234–244. https://doi.org/10.1016/j.ifset.2016.07.005

Ali, M. Y., Sina, A. A. I., Khandker, S. S., Neesa, L., Tanvir, E. M., Kabir, A., … Gan, S. H. (2020). Nutritional composition and bioactive compounds in tomatoes and their impact on human health and disease: A review. *Foods, 10*(1), 45. https://doi.org/10.3390/foods10010045

Aoac. (2012). *Official Methods of Analysis* ((19th ed.).). Association of Official Analytical Chemists.

Ayón-Reyna, L. E., González-Robles, A., Rendón-Maldonado, J. G., Báez-Flores, M. E., López-López, M. E., & Vega-García, M. O. (2017). Application of a hydrothermal-calcium chloride treatment to inhibit postharvest anthracnose development in papaya. *Postharvest Biology and Technology, 124*, 85–90. https://doi.org/10.1016/j.postharvbio.2016.10.009

Besada, C., Llorca, E., Novillo, P., Hernando, I., & Salvador, A. (2015). Short-term high CO2 treatment alleviates chilling injury of persimmon cv. Fuyu by preserving the parenchyma structure. *Food Control, 51*, 163–170. https://doi.org/10.1016/j.foodcont.2014.11.013

Biswas, P., East, A. R., Brecht, J. K., Hewett, E. W., & Heyes, J. A. (2012). Intermittent warming during low temperature storage reduces tomato chilling injury. *Postharvest Biology and Technology, 74*, 71–78. https://doi.org/10.1016/j.postharvbio.2012.07.002

Cáez Ramírez, G., Téllez-Medina, D. I., García-Armenta, E., & -López, G. F. G.. (2017). Digital image analysis and fractal metrics as potential tools to monitor colour changes in fresh-cut papaya (Carica papaya L.). *International Journal of Food Properties, 20*, S177–S189. https://doi.org/10.1080/10942912.2017.1293090

Cantre, D., Herremans, E., Verboven, P., Ampofo-Asiama, J., Hertog, M. L. A. T. M., & Nicolaï, B. M. (2017). Tissue breakdown of mango (Mangifera indica L. cv. Carabao) due to chilling injury. *Postharvest Biology and Technology, 125*, 99–111. https://doi.org/10.1016/j.postharvbio.2016.11.009

Cárdenas-Pérez, S., Chanona-Pérez, J. J., Méndez-Méndez, J. V., Calderón-Domínguez, G., López-Santiago, R., & Arzate-Vázquez, I. (2016). Nanoindentation study on apple tissue and isolated cells by atomic force microscopy, image and fractal analysis. *Innovative Food Science & Emerging Technologies, 34*, 234–242. https://doi.org/10.1016/j.ifset.2016.02.004

Carvajal, F., Palma, F., Jamilena, M., & Garrido, D. (2015). Cell wall metabolism and chilling injury during postharvest cold storage in zucchini fruit. *Postharvest Biology and Technology, 108*, 68–77. https://doi.org/10.1016/j.postharvbio.2015.05.013

Cruz-Mendívil, A., López-Valenzuela, J. A., Calderón-Vázquez, C. L., Vega-García, M. O., Reyes-Moreno, C., & Valdez-Ortiz, A. (2015). Transcriptional changes associated with chilling tolerance and susceptibility in 'Micro-Tom' tomato fruit using RNA-Seq. *Postharvest Biology and Technology, 99*, 141–151. https://doi.org/10.1016/j.postharvbio.2014.08.009

da Fonseca de Albuquerque, M., Bastos, D., Ţălu, Ş., Matos, R., Pires, M., Salerno, M., da Fonseca Filho, H., & Simão, R. (2022). Vapor Barrier Properties of Cold Plasma Treated Corn Starch Films. *Coatings, 12*(7), 1006. 10.3390/coatings12071006.

Ding, Y., Shi, Y., & Yang, S. (2019). Advances and challenges in uncovering cold tolerance regulatory mechanisms in plants. *New Phytologist, 222*(4), 1690–1704. https://doi.org/10.1111/nph.15696

Erkan, M., Pekmezci, M., & Wang, C. Y. (2005). Hot water and curing treatments reduce chilling injury and maintain post-harvest quality of "Valencia" oranges. *International Journal of Food Science and Technology, 40*(1), 91–96. https://doi.org/10.1111/j.1365-2621.2004.00912.x

Espinosa-Velázquez, R., Dorantes-Alvarez, L., Gutiérrez-López, G. F., García-Armenta, E., Sánchez-Segura, L., Perea-Flores, M. J., … Ortíz-Moreno, A. (2016). Morpho-structural description of unripe and ripe avocado pericarp (Persea americana Mill var. *Drymifolia). Revista Mexicana de Ingeniería Química, 15*(2), 469–480.

García-Armenta, E., & Gutiérrez-López, G. F. (2022). Fractal Microstructure of Foods. *Food Engineering Reviews, 14*(1), 1–19. https://doi.org/10.1007/s12393-021-09302-y

García-Armenta, E., Gutiérrez-López, G. F., Hernández-Sánchez, H., & Alamilla-Beltrán, L. (2019). Characterisation of the global breakage pattern of maltodextrin agglomerates. *Powder Technology, 343*, 362–365. https://doi.org/10.1016/j.powtec.2018.11.064

García-Armenta, E., Picos-Corrales, L. A., Gutiérrez-López, G. F., Gutiérrez-Dorado, R., Perales-Sánchez, J. X. K., García-Pinilla, S., … Armenta-Manjarrez, M. A. (2021). Preparation of surfactant-free emulsions using amaranth starch modified by reactive extrusion. *Colloids and Surfaces A: Physicochemical and Engineering Aspects, 608*, Article 125550. https://doi.org/10.1016/j.colsurfa.2020.125550

García-Armenta, E., Téllez-Medina, D. I., Alamilla-Beltrán, L., Arana-Errasquín, R., Hernández-Sánchez, H., & Gutiérrez-López, G. F. (2014). Multifractal breakage patterns of thick maltodextrin agglomerates. *Powder Technology, 266*, 440–446. https://doi.org/10.1016/j.powtec.2014.06.047

Ge, W., Kong, X., Zhao, Y., Wei, B., Zhou, Q., & Ji, S. (2019). Insights into the metabolism of membrane lipid fatty acids associated with chilling injury in post-harvest bell peppers. *Food Chemistry, 295*, 26–35. https://doi.org/10.1016/j.foodchem.2019.05.117

Habibi, F., Ramezanian, A., Guillén, F., Martínez-Romero, D., Serrano, M., & Valero, D. (2020). Susceptibility of blood orange cultivars to chilling injury based on antioxidant system and physiological and biochemical responses at different storage temperatures. *Foods, 9*(11), 1609. https://doi.org/10.3390/foods9111609

Huang, H., Wang, L., Qiu, D., Zhang, N., & Bi, F. (2021). Changes of Morphology, Chemical Compositions, and the Biosynthesis Regulations of Cuticle in Response to Chilling Injury of Banana Fruit During Storage. *Frontiers in Plant Science, 12*, Article 792384. https://doi.org/10.3389/fpls.2021.792384

Imahori, Y., Bai, J., & Baldwin, E. (2016). Antioxidative responses of ripe tomato fruit to postharvest chilling and heating treatments. *Scientia Horticulturae, 198*, 398–406. https://doi.org/10.1016/j.scienta.2015.12.006

Jha, P. K., Xanthakis, E., Chevallier, S., Jury, V., & Le-Bail, A. (2019). Assessment of freeze damage in fruits and vegetables. *Food Research International, 121*, 479–496. https://doi.org/10.1016/j.foodres.2018.12.002

Jung, H., & Yoon, W. B. (2017). Multifractal approaches of the ring tensile rupture patterns of dried laver (Porphyra) as affected by the relative humidity. *Journal of Food Science, 82*(12), 2894–2900. https://doi.org/10.1111/1750-3841.13942

Khodabakhshian, R., & Baghbani, R. (2021). Classification of bananas during ripening using peel roughness analysis—An application of atomic force microscopy to food process. *Journal of Food Process Engineering, 44*(11), e13857.

Kong, X., Ge, W., Wei, B., Zhou, Q., Zhou, X., Zhao, Y., & Ji, S. (2020). Melatonin ameliorates chilling injury in green bell peppers during storage by regulating membrane lipid metabolism and antioxidant capacity. *Postharvest Biology and Technology, 170*, Article 111315. https://doi.org/10.1016/j.postharvbio.2020.111315

Lares-Michel, M., Housni, F. E., Aguilera Cervantes, V. G., Nava, R. M. M., Del Toro, H. B., Cañedo, B., … del Carmen Carmona, M. (2018). The Relationship between Consumption, Socioeconomic Level and Reasons of Tomato Intake in Mexico. *Agricultural Sciences, 09*(07), 777–791. https://doi.org/10.4236/as.2018.97055

Li, X., Yun, J., Fan, X., Xing, Y., & Tang, Y. (2011). Effect of 1-methylcyclopropene and modified atmosphere packaging on chilling injury and antioxidative defensive mechanism of sweet pepper. *African Journal of Biotechnology, 10*(34), 6581–6589.

Liu, J., Li, F., Li, T., Yun, Z., Duan, X., & Jiang, Y. (2019). Fibroin treatment inhibits chilling injury of banana fruit via energy regulation. *Scientia Horticulturae, 248*, 8–13. https://doi.org/10.1016/j.scienta.2018.12.052

Loayza, F. E., Brecht, J. K., Simonne, A. H., Plotto, A., Baldwin, E. A., Bai, J., & Lon-Kan, E. (2021). A brief hot-water treatment alleviates chilling injury symptoms in fresh tomatoes. *Journal of the Science of Food and Agriculture, 101*(1), 54–64. https://doi.org/10.1002/jsfa.10821

López-Velázquez, J. G., Delgado-Vargas, F., López-Ángulo, G., García-Armenta, E., López-López, M. E., Ayón-Reyna, L. E., … Vega-García, M. O. (2020). Phenolic profile associated with chilling tolerance induced by the application of a hot water treatment in bell pepper fruit. *Journal of Food Science, 85*(7), 2080–2089. https://doi.org/10.1111/1750-3841.15310

Matos, R. S., Pinto, E. P., Pires, M. A., Ramos, G. Q., Ţălu, Ş., Lima, L. S., & da Fonseca Filho, H. D. (2023). Evaluating the roughness dynamics of kefir biofilms grown on Amazon cupuaçu juice: A monofractal and multifractal approach. *Microscopy, dfad040*. https://doi.org/10.1093/jmicro/dfad040

Matos, R. S., Ţălu, Ş., Mota, G. V. S., Pinto, E. P., Pires, M. A., Abraçado, L. G., & Ferreira, N. S. (2021). Correlating structure and morphology of Andiroba leaf (Carapa guianensis Aubl.) by microscopy and fractal theory analyses. *Applied Sciences, 11*(13), 5848. https://doi.org/10.3390/app11135848

Pan, Y., Zhang, S., Yuan, M., Song, H., Wang, T., Zhang, W., & Zhang, Z. (2019). Effect of glycine betaine on chilling injury in relation to energy metabolism in papaya fruit during cold storage. *Food Science & Nutrition, 7*(3), 1123–1130. https://doi.org/10.1002/fsn3.957

Phothiset, S., & Charoenrein, S. (2014). Effects of freezing and thawing on texture, microstructure and cell wall composition changes in papaya tissues. *Journal of the Science of Food and Agriculture, 94*(2), 189–196. https://doi.org/10.1002/jsfa.6226

Pristijono, P., Bowyer, M. C., Scarlett, C. J., Vuong, Q. V., Stathopoulos, C. E., & Golding, J. B. (2018). Combined postharvest UV-C and 1-methylcyclopropene (1-MCP) treatment, followed by storage continuously in low level of ethylene atmosphere improves the quality of Tahitian limes. *Journal of Food Science and Technology, 55*(7), 2467–2475. https://doi.org/10.1007/s13197-018-3164-4

Rasouli, M., Koushesh Saba, M., & Ramezanian, A. (2019). Inhibitory effect of salicylic acid and Aloe vera gel edible coating on microbial load and chilling injury of orange fruit. *Scientia Horticulturae, 247*, 27–34. https://doi.org/10.1016/j.scienta.2018.12.004

Sandoval-Ceballos, M. G., Kalungwana, N. A., Griffin, J. H. C., Martínez-Guerra, G., Ramírez-Ramírez, I., Maldonado-Peralta, R., … Toledo-Ortiz, G. (2021). The importance of conserving Mexico's tomato agrodiversity to research plant biochemistry under different climates. *Plants, People, Planet, 3*(6), 703–709. https://doi.org/10.1002/ppp3.10218

Serrano, S., Perán, F., Gutiérrez de Ravé, E., Cumplido, A., & Jiménez-Hornero, F. J. (2019). Multifractal analysis application to the study of fat and its infiltration in Iberian ham: Influence of racial and feeding factors and type of slicing. *Meat Science, 148*, 55–63. https://doi.org/10.1016/j.meatsci.2018.10.004

Serrano, S., Perán, F., Jiménez-Hornero, F. J., & Gutiérrez de Ravé, E. (2013). Multifractal analysis application to the characterization of fatty infiltration in Iberian and White pork sirloins. *Meat Science, 93*(3), 723–732. https://doi.org/10.1016/j.meatsci.2012.11.015

Song, C., Wang, K., Xiao, X., Liu, Q., Yang, M., Li, X., … Yang, Z. (2022). Membrane lipid metabolism influences chilling injury during cold storage of peach fruit. *Food Research International, 157*, Article 111249. https://doi.org/10.1016/j.foodres.2022.111249

Starodubtseva, M. N., Starodubtsev, I. E., & Starodubtsev, E. G. (2017). Novel fractal characteristic of atomic force microscopy images. *Micron, 96*, 96–102. https://doi.org/10.1016/j.micron.2017.02.009

Ţălu, Ş., Stach, S., Solaymani, S., Moradian, R., Ghaderi, A., Hantehzadeh, M. R., … Izadyar, S. (2015). Multifractal spectra of atomic force microscope images of Cu/Fe nanoparticles based films thickness. *Journal of Electroanalytical Chemistry, 749*, 31–41. https://doi.org/10.1016/j.jelechem.2015.04.009

Tilahun, S., Park, D. S., Solomon, T., Choi, H. R., & Jeong, C. S. (2019). Maturity stages affect nutritional quality and storability of tomato cultivars. *CyTA - Journal of Food, 17*(1), 87–95. https://doi.org/10.1080/19476337.2018.1554705

Valenzuela-Lagarda, J. L., García-Armenta, E., Pacheco-Aguilar, R., Gutiérrez-Dorado, R., Mazorra-Manzano, M.Á., Lugo-Sánchez, M. E., & Muy-Rangel, M. D. (2018). Relationships between morphometrical properties and the texture of an extrusion-expanded snack made from squid mantle (Dosidicus gigas). *Journal of Texture Studies, 49*(5), 476–484. https://doi.org/10.1111/jtxs.12321

Vega-García, M. O., López-Espinoza, G., Ontiveros, J. C., Caro-Corrales, J. J., Vargas, F. D., & López-Valenzuela, J. A. (2010). Changes in protein expression associated with chilling injury in tomato fruit. *Journal of the American Society for Horticultural Science, 135*(1), 83–89. https://doi.org/10.21273/JASHS.135.1.83

Venkatachalam, K. (2018). Exogenous nitric oxide treatment impacts antioxidant response and alleviates chilling injuries in longkong pericarp. *Scientia Horticulturae, 237*, 311–317. https://doi.org/10.1016/j.scienta.2018.04.032

Wang, H., Wang, J., Mujumdar, A. S., Jin, X., Liu, Z.-L., Zhang, Y., & Xiao, H.-W. (2021). Effects of postharvest ripening on physicochemical properties, microstructure, cell wall polysaccharides contents (pectin, hemicellulose, cellulose) and nanostructure of kiwifruit (Actinidia deliciosa). *Food Hydrocolloids, 118*, Article 106808. https://doi.org/10.1016/j.foodhyd.2021.106808

Yaşar, F., & Akgünlü, F. (2005). Fractal dimension and lacunarity analysis of dental radiographs. *Dentomaxillofacial Radiology, 34*(5), 261–267. https://doi.org/10.1259/dmfr/85149245

Zhang, M., Liu, W., Li, C., Shao, T., Jiang, X., Zhao, H., & Ai, W. (2019). Postharvest hot water dipping and hot water forced convection treatments alleviate chilling injury for zucchini fruit during cold storage. *Scientia Horticulturae, 249*, 219–227. https://doi.org/10.1016/j.scienta.2019.01.058

Zhu, Z., Ding, Y., Zhao, J., Nie, Y., Zhang, Y., Sheng, J., & Tang, X. (2016). Effects of postharvest gibberellic acid treatment on chilling tolerance in cold-stored tomato (Solanum lycopersicum L.) fruit. *Food and Bioprocess Technology, 9*(7), 1202–1209. https://doi.org/10.1007/s11947-016-1712-3